High-Pressure Electrical Transport Measurements on 2*H*-$NbSe_2$ Thin Films

Meilun Li[1], Chao Jiang[1], Yinshang Liu[2], Dong Wang[1], Chi Zhang[2], Tao Hu[3], ChuanLong Lin[1†], Yang Ding[1], Wenge Yang[1], Ho-Kwang Mao[1], and Hong Xiao[1*]
[1] *Center for High Pressure Science and Technology Advanced Research, Beijing, 100193, China*
[2] *Beijing Academy of Quantum Information Science, Beijing, 100193, China and*
[3] *Guangdong University of Science and Technology, Dongguan, 523083, China*
(Dated: September 25, 2026)

Ultrathin 2*H*-$NbSe_2$ exhibits a unique interplay of an enhanced charge density wave (CDW) and Ising-type superconductivity, making it a promising candidate for quantum tuning studies. Hydrostatic pressure, applied via diamond anvil cells (DACs) is widely employed to explore the physical properties of materials. However, high-pressure measurements have never been performed on $NbSe_2$ thin films due to the technical challenges associated with transport measurements in DACs. Here, we introduce a technique combining pre-patterned electrodes and a dry-transfer process to enable precise electrical transport measurements on two-dimensional (2D) materials under pressure. Using this approach, we measured resistance, magnetoresistance, and Hall effect in $NbSe_2$ thin films under high pressure. The CDW transition temperature (T_{CDW}) is enhanced compared to the bulk $NbSe_2$, verifying the ultrathin nature of the samples. Despite the enhanced T_{CDW} in thin films, the CDW order vanishes near $\sim$ 5 GPa, similar as the bulk $NbSe_2$. In addition, two superconducting regions are observed in thin film $NbSe_2$ under pressure, with the optimal superconducting transition temperature (T_c) achieved near $\sim$ 5 GPa, significantly lower than the pressure required in bulk samples. The CDW ending at the maximum T_c suggests that the superconducting order in ultrathin $NbSe_2$ competes with CDW order. Our work establishes a novel method for electrical transport measurements in nanometer-thin films under pressure and reports the first high-pressure data on thin-film $NbSe_2$, shedding new insights on the interplay of competing orders in 2D quantum materials.

Keywords: 2*H*-$NbSe_2$; Thin films; High pressure; Superconductivity; Charge-density wave
PACS: 74.70.Xa, 74.25.Fy, 74.62.Fj, 71.45.Lr

I. INTRODUCTION

The groundbreaking work of Geim and Novoselov in isolating monolayer graphene through mechanical exfoliation in 2004 [1] marked the beginning of a transformative era in the exploration of two-dimensional (2D) materials. Reducing materials from bulk to thin films or monolayers has unveiled a range of novel properties, such as zero bandgap [2] and high mobility [3] in graphene, the highly tunable superconductivity in 2D systems [4–9] , and the discovery of 2D Ising superconductivity in monolayers of $NbSe_2$ [10] and MoS_2 [9]. Other notable findings include layer-dependent magnetism in 2D magnetic materials [11] and the topological quantum spin Hall effect in monolayers [12].

Among 2D materials, the transition metal dichalcogenide (TMD) family offers a wealth of intriguing properties. The 2*H*-$NbSe_2$ system is particularly notable for its rich physics [13–18], including an incommensurate charge density wave (CDW) transition at $T_{CDW} = 33.5$ K [19] and superconducting transition at $T_c = 7.2$ K [20]. In bulk $NbSe_2$, T_c exhibits a dome-like dependence on pressure, peaking before gradually decreasing [21]. The reduction of $NbSe_2$ to few layers further modifies its properties: Notably, the Ising type superconductivity is observed in the few-layer sample; T_c decreases while T_{CDW} increases, reaching 3.1 K and 145 K, respectively, in the monolayer [22].

Pressure, as a 'pure' tuning parameter, introduces no chemical impurities, making it a powerful tool for modulating material properties in combination with dimensional control to uncover new physical phenomena. Diamond anvil cells (DACs) are a standard device for applying high pressure. In 1981, Mao et al. developed a method for electrical transport measurements under pressure using the conventional four-lead technique [23], which was restricted to bulk or powdered samples. Subsequent advancements integrated conductive electrodes with diamond anvils [24–31], simplifying the manual bonding process and enabling thin-layer sample measurements. Electrodes are often fabricated by photolithography on diamond followed by Ti/Au vapor deposition [32–35], but this approach presents challenges, including achieving precise flatness on the diamond culet, alignment issues during mask-based lithography, and the time-consuming nature of preparing new patterns for each experiment. To address these limitations, direct laser writing (DLW) is proposed to fabricate electrode patterns without photolithography masks [36, 37]. While DLW simplifies some aspects, it does not entirely resolve the challenges, highlighting the need for a more efficient and practical method for electrical transport measurements in thin-film samples under pressure.

Despite extensive studies of bulk and ambient thin-layer $NbSe_2$, the behavior of thin-layer $NbSe_2$ under pressure remains unexplored. In this work, we introduce a novel method for electrical transport measurements in thin films under pressure. Pre-patterned electrodes are transferred onto thin flakes using a polyvinyl alcohol (PVA) film, and the entire assembly is subsequently transferred onto a diamond anvil for measurements. Systematic studies of thin-film $NbSe_2$ under pressure re-

vealed intriguing differences in how superconductivity and CDW phases respond to pressure. Our data show that in thin film $NbSe_2$, the CDW order vanishes near $\sim$ 5 GPa, similar as in bulk $NbSe_2$, however, the optimal T_c is obtained at a pressure which is much lower than the pressure needed in bulk samples. Two superconducting regions are observed in thin film $NbSe_2$, and the pressure at which T_c is a maximum coincident with the pressure where CDW order collapses.

II. EXPERIMENTAL DETAILS

We have developed a high efficiency strategy for performing electrical transport measurements on 2D thin-film materials under pressure. Techniques such as laser writing [36] or photolithography [32] can introduce unwanted stress, defects, or micro-cracks into the diamond, potentially compromising its mechanical strength and increasing the likelihood of failure under the extreme pressures used in DACs. In our method we transfer pre-patterned gold electrodes onto thin film samples using polyvinyl alcohol (PVA) films to create reliable electrical contact [38, 39], the entire assembly is then transferred onto the diamond culet inside the DAC using a flexible transfer technique. This approach avoids stress on the diamond and simplifies the process, maintaining the integrity of the sample-electrode interface.

Figure 1 illustrates the steps. (a) Fabrication of Au Electrodes: The Au electrode patterns are fabricated on Si/SiO_2 substrate using ultraviolet lithography and metal thermal evaporation technology. To protect the gold electrodes, a polyvinyl alcohol (PVA) layer is applied as a protective coating. (b) Fabrication of $NbSe_2$ Thin Flakes: Thin flakes of $NbSe_2$ are exfoliated from the bulk single crystal using scotch tape. The surface of the Si/SiO_2 substrate is cleaned using a plasma before processing it onto the $NbSe_2$ flakes. (c) Attachment of $NbSe_2$ Thin Flakes to Au Electrodes: A strip of Au/PVA is affixed to a polydimethylsiloxane (PDMS) layer mounted on a glass slide. The Au/PVA strip is aligned with a $NbSe_2$ thin flake using a sample transfer stage under a microscope and then baked. (d) Transfer of the Sample and Au Electrodes to the Diamond Culet: Using a transfer platform under a microscope, the $NbSe_2$/Au/PVA/PDMS assembly on the glass slide is positioned precisely at the center of the diamond culet and tightly fitted. Then the top PDMS is detached and the PVA is washed away. (e) Gasket Preparation: To insulate electrodes from the metallic gasket, a mixture of cubic boron nitride (BN) and epoxy was compressed into the indentation area of a BeCu gasket. The exposed parts on the underside of the gasket are coated with Stycast 2850FT BK. (f) Encapsulation: After carefully assembling the components, the diamond anvil cell is sealed to encapsulate the sample and electrodes.

$NbSe_2$ used in this work is commercially sourced from Hefei-Kejing and HQ. The structural and compositional properties of the bulk crystals were characterized prior to exfoliation. Single-crystal X-ray diffraction (XRD) measurement was performed at 296 K on a Bruker D8 VENTURE diffractometer equipped with Ag $K\alpha$ radiation (λ = 0.56086 Å). Absorption corrections were applied using the multi-scan method with SADABS [40, 41]. The crystal structure was solved by the intrinsic phasing method with SHELXT [42] and refined against F^2 by full-matrix least-squares fitting with SHELXL [43], as implemented in the APEX4 software package (Bruker AXS). Scanning electron microscopy (SEM) and energy-dispersive X-ray spectroscopy (EDS) analyses were performed using a JSM-7900F thermal field emission SEM, which offers an ultra-high resolution of up to 0.6 nm at 15 kV. For ambient-pressure samples, the layer number of the flakes was determined using atomic force microscopy (AFM). For samples in the DAC, the thickness was estimated from calibrated optical contrast and cross-checked with the thickness dependence of T_c and T_{CDW}. A diamond anvil cell (DAC) made of CuBe alloy, with a diamond anvil culet of 500 μm, was employed to apply pressure to $NbSe_2$ thin films. Simultaneous measurements of resistance and Hall resistance were performed using the van der Pauw method [44]. Electrical transport data was collected using a Quantum Design Physical Property Measurement System (PPMS). Silicone oil was used as the pressure transmission medium to ensure hydrostatic conditions. Pressure calibration was carried out using Ruby fluorescence shift measurements at room temperature.

III. RESULTS AND DISCUSSION

To guide the reader through our results, we briefly summarize the content of each figure here. Figure 2 presents the structural and compositional characterization of the bulk $NbSe_2$ crystal. Figure 3 shows the evolution of superconductivity in the thin film under pressure. Figure 4 and 5 report the magnetoresistance and Hall effect measurements on thin film, respectively. Figure 6 summarizes the temperature–pressure phase diagram. Figure 7 illustrates how RRR influences electrical transport properties.

We begin by discussing the structural and compositional analysis of the bulk $NbSe_2$ crystals. Figure 2(a) displays an optical image of the crystal, revealing a shiny, layered morphology characteristic of high-quality single crystals. At ambient pressure, we performed x-ray diffraction measurements on a single-crystal sample of bulk $NbSe_2$. The refinement confirms that the crystal adopts the hexagonal space group $P6_3/mmc$, with lattice parameters a = 3.446 (2) Å, c = 12.535 (9) Å. The crystal structure was visualized using the VESTA [45], as shown in Fig. 2(b). Figure 2(c) compares the observed and calculated diffraction intensities, showing excellent agreement and validating the structural model. Figure 2(d) presents the processed diffraction spots in the (hk0) plane of reciprocal space, confirming the high crystallinity and well-defined orientation of the

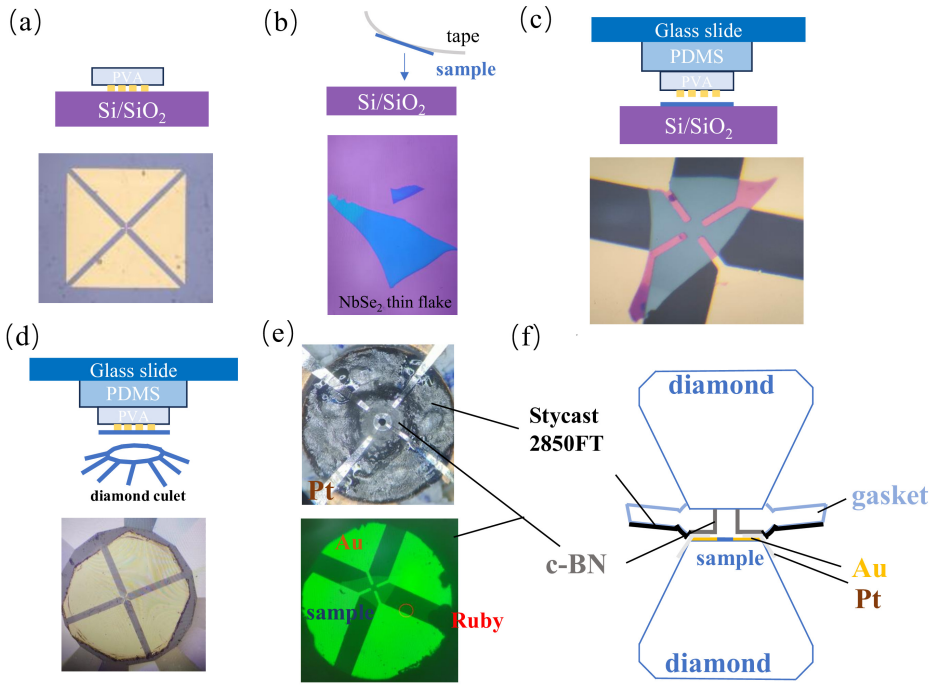


FIG. 1. Implementation of 2D thin flake sample inside a DAC. (a) Fabrication of Au electrodes. (b) Fabrication of $NbSe_2$ thin flakes. (c) Attachment of thin flake sample to Au electrodes. (d) Transfer of the sample and Au electrodes to the diamond culet. (e) Gasket preparation. (f) Encapsulation.

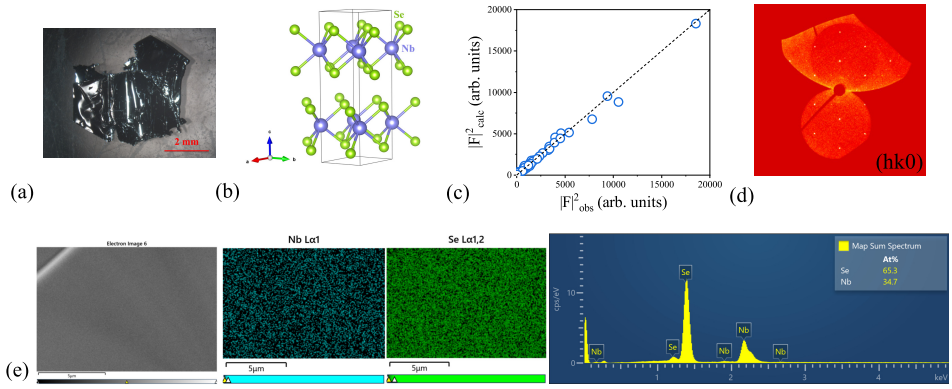


FIG. 2. (a) Optical image of $NbSe_2$ single crystal. (b) Crystal structure of $NbSe_2$ determined by single crystal refinement; the picture is drawn by VESTA software. (c) Comparison between observed and calculated XRD intensities, confirming structural refinement quality. (d) Diffraction pattern in the (hk0) plane of reciprocal space. (e) SEM image and EDS elemental maps.

sample. To further assess the sample quality, scanning electron microscopy (SEM) and energy-dispersive X-ray spectroscopy (EDS) were performed, as shown in Fig. 2(e). The SEM image reveals atomically flat surfaces with a clear layered structure, while the EDS elemental maps confirm a uniform spatial distribution of Nb and Se without detectable impurities. These results demonstrate that the $NbSe_2$ crystals used in this study exhibit excellent structural integrity and compositional homogeneity.

Figure 3(a) presents the temperature T dependent resistance R curves of device S1 under various pressures, P = 1.4, 2.0, 2.7, 4.0, 5.0, 6.1, 7.6, 9.4, 10.9, 12.2, 13.8, 15.8, 17.5, 19.3, 22.6 and 25.5 GPa. The superconducting transition temperature T_c is determined by the intersection of the two straight lines, as shown in Fig. 3(b). The superconductivity in $NbSe_2$ thin film persists across the entire pressure range investigated. The resistance curves remain smooth at all pressures, with zero resistance observed after the superconducting transition. This indicates perfect ohmic contact between the sample and electrodes, which is stable up to the highest pressure of 25.5 GPa. The sudden drop in resistance is also sensitive to the applied magnetic field, with T_c decreasing

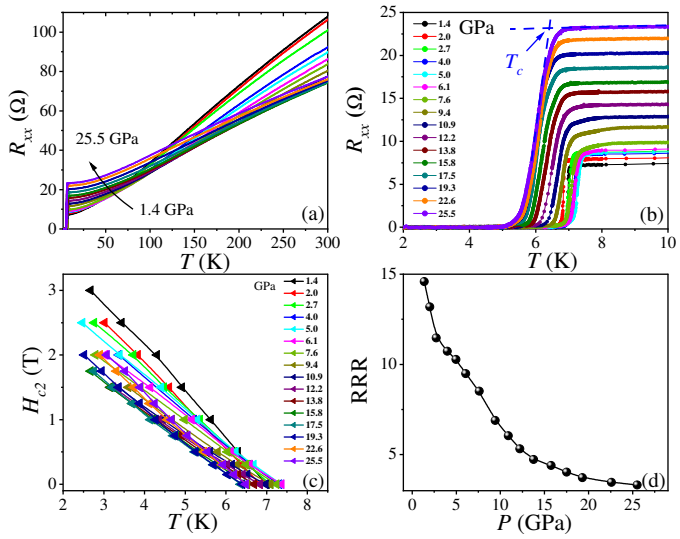


FIG. 3. (a) Temperature (T) dependence of resistance (R) at different pressures, P = 1.4, 2.0, 2.7, 4.0, 5.0, 6.1, 7.6, 9.4, 10.9, 12.2, 13.8, 15.8, 17.5, 19.3, 22.6 and 25.5 GPa. (b) The enlarged superconducting transitions. (c) The temperature dependence of the upper critical field H_{c2} at different pressures. (d) RRR vs P.

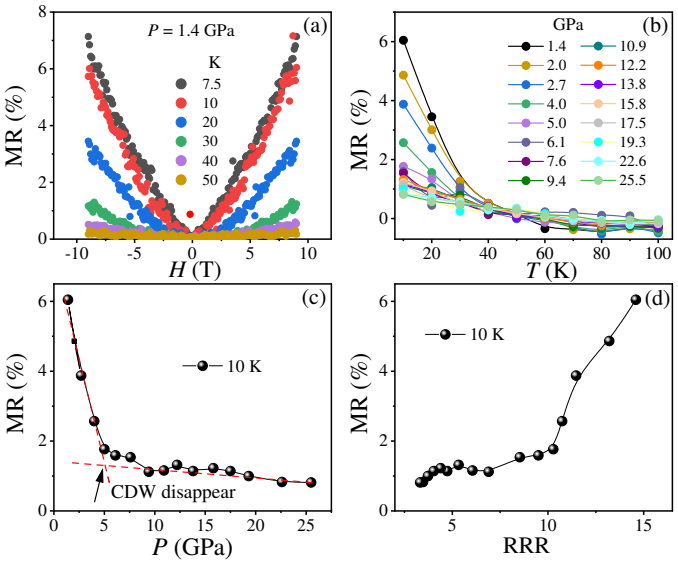


FIG. 4. (a) The H dependence of the magnetoresistance MR =[R(9 T) - R(0 T)]/R(0 T) × 100 % at 1.4 GPa. (b) The temperature dependence of the MR at different pressures P = 1.4, 2.0, 2.7, 4.0, 5.0, 6.1, 7.6, 9.4, 10.9, 12.2, 13.8, 15.8, 17.5, 19.3, 22.6 and 25.5 GPa. (c) MR vs P at T = 10 K. (d) MR vs RRR at T = 10 K.

as the magnetic field increases. This confirms that the observed transitions are superconducting in nature and not due to electrode failure at low temperatures, further validating the quality of our electrodes. A second independent device (S2), measured up to 4 GPa, shows similar behavior and a consistent $T_c(P)$ evolution (Fig. A1), confirming the reproducibility of our results. Figure 3(c) depicts the temperature dependence of upper critical field H_{c2} under different pressures. The data reveal an approximately linear relationship between H_{c2} and T_c. The temperature-pressure T - P phase diagram of $NbSe_2$ thin film is summarized in Fig. 6(b).

The superconducting phase displays two regions, which is not found in bulk $NbSe_2$ under pressure [Fig. 6(b)]. T_c first increases with pressure, reaching a maximum value at $P \sim 5$ GPa and then decreases with further increasing pressure. At $P \sim 19.3$ GPa, T_c reaches a dip before increasing slightly. Superconductivity persists up to the highest pressure of 25.5 GPa explored in this study. The optimal T_c of $\sim$ 7.4 K is achieved at $\sim$ 5 GPa in the thin film sample, contrasting with bulk $NbSe_2$, where the optimal T_c occurs at much higher pressures, $\sim$ 10 GPa in Ref. [21] and $\sim$ 17.8 GPa in Ref. [46], respectively. The residual resistivity ratio RRR($\equiv R(300\ \mathrm{K})/R(10\ \mathrm{K})$) decreases with increasing pressure [Fig. 3(d)], implying a pressure enhanced disorder in $NbSe_2$ samples.

Figure 4(a) shows the H dependence of in-plane magnetoresistance MR with magnetic field along the c axis for 7.5, 10, 20, 30, 40 and 50 K at 1.4 GPa. At a fixed pressure, decreasing temperature reveals an MR upturn that gradually diminishes with increasing pressure, as shown in Fig. 4(b). The upturn in MR signals the appearance of charge density wave (CDW) order [46]. Figure 4(c) shows MR at T = 10 K, which decreases fast with pressure increasing and flattens above 5 GPa, which implies that CDW vanishes. This result is consistent with bulk $NbSe_2$, where CDW-induced features also vanish near $\sim$ 5 GPa [47]. Figure 4(d) illustrates MR as a function of the residual resistivity ratio RRR. A distinct kink around RRR = 10, corresponding to the RRR at P = 5 GPa [Fig. 3(d)], at which the CDW vanishes. This highlights a close relationship between MR, CDW and RRR.

The temperature T dependence of the Hall coefficient R_H at various pressures is shown in Fig. 5. At lower pressure, R_H slightly increases with decreasing temperature and then shows a fast drop, signaling the onset of CDW order [48, 49]. As pressure increases, the hump (T_{CDW}) shifts to lower temperatures, and disappears near $\sim$ 5 GPa [Fig. 5(a)], consistent with the suppression of CDW order observed in bulk $NbSe_2$ [47]. Notably, as pressure exceeds $\sim$20 GPa, R_H shows a noticeable deviation from its behavior at lower pressures, including a clear sign reversal. This observation suggests a fundamentally different superconducting state in the high-pressure regime, likely associated with a reconstructed Fermi surface or a change in the dominant carrier type. Nevertheless, we cannot exclude other possible contributions, such as multiband transport, shifting carrier mobilities or changing scattering mechanisms.

Figure 6(a) shows the pressure dependence of T_{CDW}. For both bulk (from literature) and thin film samples (from this work), T_{CDW} is rapidly suppressed with increasing pressure, vanishing near $\sim$ 5 GPa. We further

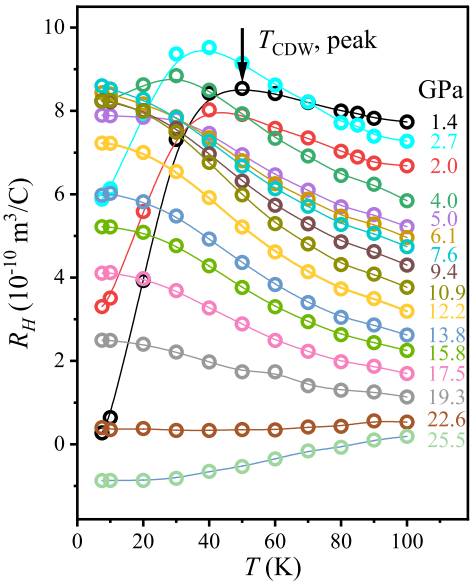


FIG. 5. The Hall coefficient R_H vs temperature at different pressures.

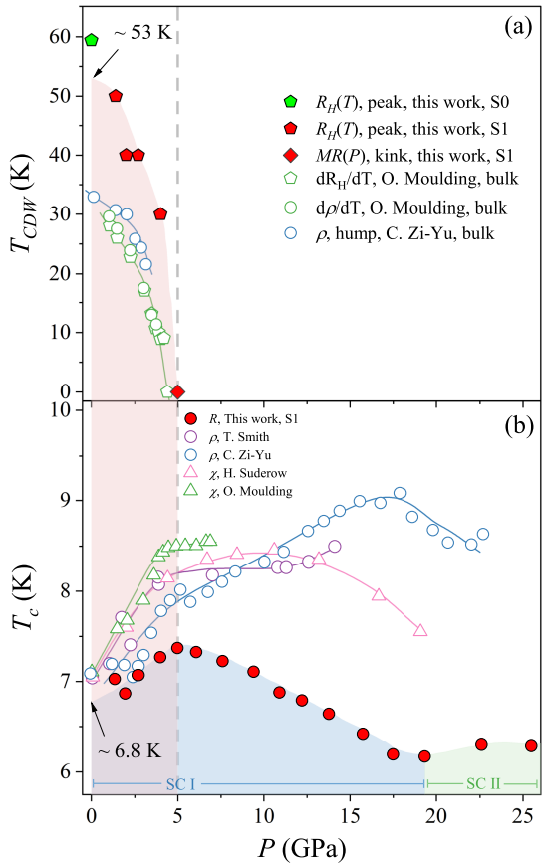


FIG. 6. Temperature vs pressure ($T - P$) phase diagram for $NbSe_2$. (a) T_{CDW} vs P. (b) T_c vs P. Solid symbols represent thin film sample data (from this work) and open symbols are data for bulk $NbSe_2$ (from literature [21, 46, 47, 52].)

compare the thickness dependence of T_{CDW} using two thin-film samples, S0 and S1. Sample S0 was measured at ambient condition, while S1 was tested under pressure. T_{CDW} is 59.4 K for sample S0 (15 nm thick) at ambient pressure. While the exact thickness of S1 in the diamond anvil cell (DAC) cannot be directly measured, its color suggests that it is thicker than S0. The results indicate T_{CDW} (S0) > T_{CDW} (S1) > T_{CDW} (bulk), consistent with previous reports that T_{CDW} increases as $NbSe_2$ thickness decreases [22]. Extrapolating thin film sample S1 data to ambient pressure, the estimated $T_c^{extra} = 6.8$ K and the $T_{CDW}^{extra} = 53$ K, suggests that S1 consists of approximately 30 layers [22]. Given a monolayer thickness of 0.6 - 0.63 nm[50, 51], this estimate yields a total thickness of 18 - 19 nm, confirming that S1 is thicker than S0.

Figure 6(b) shows T_c vs P. For the thin film sample S1, T_c increases with pressure, reaching a maximum, then decreases, showing a dip near 19.3 GPa and enters a second superconducting region as supported by the Hall coefficient data. In particular, the optimal T_c for thin film is achieved at $\sim$ 5 GPa, which is much lower than the pressure required for bulk $NbSe_2$, where optimal T_c occurs at higher pressures. This indicates that the superconductivity in thin films is more sensitive to pressure modulation. Moreover, the faster decrease of T_c above 5 GPa compared to bulk $NbSe_2$ further highlights the susceptibility of 2D superconductivity to pressure tuning, likely driven by enhanced quantum phase fluctuations and interfacial strain effects.

Notably, in $NbSe_2$ thin film the optimal T_c coincides with the pressure at which the CDW order vanishes. Similar behavior has been observed in other systems, such as kagome metal CsV_3Sb_5 [53], the layered transition-metal dichalcogenides (TMDCs) 2H-TaS_2 [54] and o-TaS_3 [55], the $CaBe_2Ge_2$-type structure $LaPt_2Si_2$ [56] and $BaPt_2As_2$ [57] , the LaTSb$_2$ (T = Ag, Au, Cu) family LaAuSb$_2$ [58]. It can be understood in terms of the interplay between the CDW order and SC. In general, there are two possible interplay between charge order and superconductivity: (1) the two orders compete, with the suppression of CDW enhancing superconductivity. (2) Pressure-induced suppression of CDW order may be associated with a hidden quantum critical point within the dome shaped superconductivity phase, resulting in an optimal T_c at the pressure where the CDW vanishes [59]. Although transport measurements alone cannot unambiguously distinguish whether phase competition or quantum criticality is the primary driving force, our observations provide key insights into both scenarios. On the one hand, the normal-state resistance, fitted by $R(T) = R_0 + AT^2 + BT^5$, shows a predominantly T^2 Fermi-liquid-like behavior (Fig. A2), and the coefficient A decreases smoothly with pressure without exhibiting a pronounced divergence near 5 GPa (Fig. A3). This lack of clear non-Fermi-liquid behavior, together with the asymmetric shape of the T_c dome, is consistent with

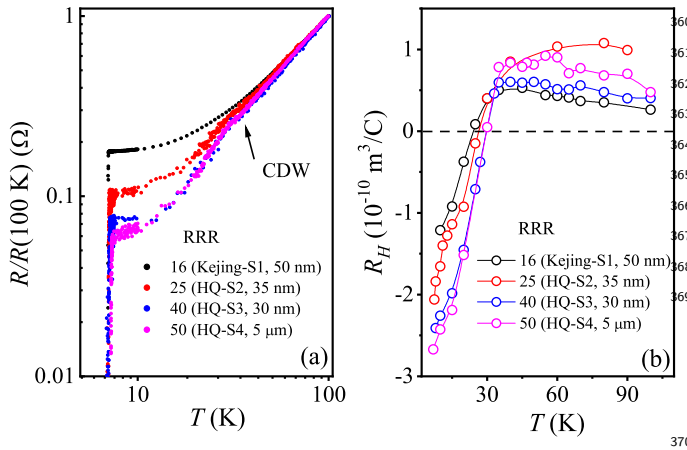


FIG. 7. (a) Resistance (R) vs temperature (T) for samples normalised to R(100 K) for different RRR($\equiv R(300\text{ K})/R(10\text{ K})$) = 16, 25, 40, 50. (b) The Hall coefficient R_H vs temperature at different RRR.

a phase-competition framework [59, 60]. On the other hand, the maximum of T_c near the vanishing of CDW order is also a hallmark of quantum criticality, where critical fluctuations may cooperate with or even drive the superconducting enhancement. Future spectroscopic or scaling studies will be necessary to further elucidate the exact roles of these two intertwined mechanisms. The coincidence of the optimal T_c with the suppression of CDW order observed in our work possibly suggests the competition scenario in ultrathin $NbSe_2$.

The observed behavior in thin film $NbSe_2$ contrasts with bulk $NbSe_2$, where optimal T_c appears at pressures significantly higher than the pressure at which the CDW order vanishes and inconsistent results have been reported [16, 46, 47, 61]. The discrepancy is possibly due to the inhomogeneities in bulk samples and pressure which obscure any intrinsic correlation between SC and CDW. In this work, we applied pressure to exfoliated ultrathin $NbSe_2$ samples using a pre-patterned method. The samples were reduced to thin layers, ensuring uniform thickness and a small measurement area. This configuration allows the samples to experience more uniform pressure compared to bulk samples. Therefore, our ultrathin samples offer a clearer and more reliable platform to study two-dimensional SC and CDW than bulk measurements. The data are consistent with a scenario involving phase competition.

Next, we examine the influence of RRR on the electrical transport properties below the T_{CDW} from two manufacturers. Samples with varying RRR values were tested. Figure 7 (a) shows the resistance-temperature (R-T) curves for samples with RRR = 16, 25, 40 and 50. No CDW transition is observed for sample with RRR = 16. However, for RRR values of 25 and above, a hump near 33 K becomes increasingly pronounced, consistent with previous report that CDW anomalies are observed when RRR exceeds 30 [62]. Figure 7(b) displays the temperature dependence of R_H for samples with different RRR values. Above ~ 30 K, R_H exhibits weak temperature dependence, but below this threshold, R_H decreases rapidly due to CDW formation. The rate of decrease accelerates with higher RRR, and R_H changes sign from positive to negative near 25 K. The sign change is related to the presence of CDW, which increases with increasing RRR, consistent with our result of pressure tuning. This behavior further underscores the interplay between CDW, RRR, and R_H.

IV. CONCLUSIONS

In summary, we have developed an efficient and cost-effective method for conducting electrical transport measurements on two-dimensional (2D) thin films under high pressure. The stability and quality of the pre-patterned electrodes were confirmed up to the highest pressure investigated (25.5 GPa). Our work represents the first high-pressure transport study of thin-film $NbSe_2$, extending beyond previous efforts that have focused solely on the bulk material. Notably, our results in thin-film samples reveal distinct responses of charge density wave (CDW) and superconducting (SC) orders to pressure compared to bulk $NbSe_2$. The CDW order is completely suppressed at pressures comparable to bulk $NbSe_2$. However, SC order in thin films reaches its optimal transition temperature T_c at significantly lower pressures and exhibits a reduced T_c value compared to the bulk material. Furthermore, our measurements uncover the existence of two distinct superconducting regions in thin film $NbSe_2$, a feature that has not been observed in bulk material. These findings provide new insights into the interplay between competing quantum orders in low-dimensional systems.

Appendix A: Reproducibility of Superconductivity under High Pressure

To confirm the reproducibility of the high-pressure superconducting phase diagram observed in device S1, high-pressure electrical transport measurements were independently conducted on a second thin film $NbSe_2$ device (S2). As shown in Figure A1(a) and A1(b), device S2 exhibits sharp superconducting transitions under hydrostatic pressure up to 4.1 GPa. Figure A1(c) compares the pressure dependence of T_c for both S1 and S2 devices over the overlapping pressure range (0-4 GPa); the superconducting transition temperature evolves with pressure similarly. These results provide additional evidence for the reproducibility and reliability of the main pressure-dependent transport behavior observed in S1.

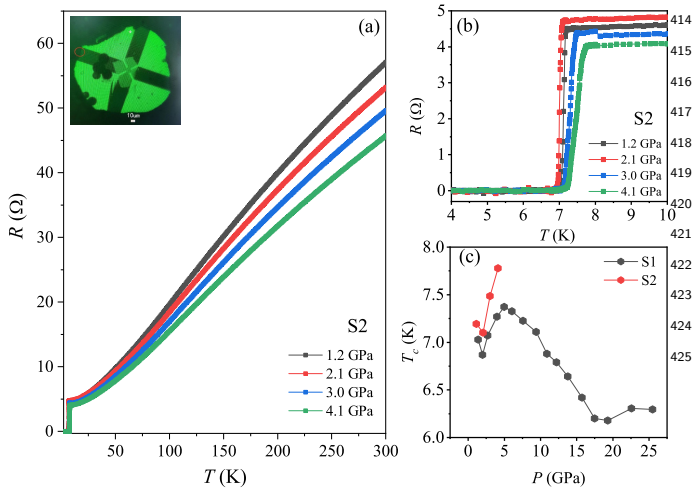


FIG. A1. Transport data for a second $NbSe_2$ device (S2). (a) R-T at 1.2-4.1 GPa; inset: optical image of the S2 device. (b) Enlarged view of $R(T)$ near T_c. (c) T_c-P comparison between S1 and S2.

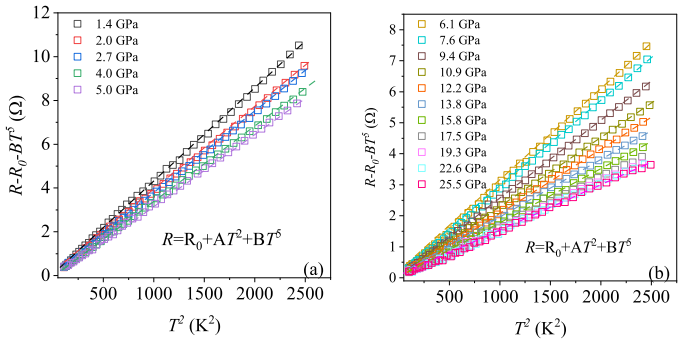


FIG. A2. Normal-state resistance analysis of thin film $NbSe_2$ under pressure. (a, b) $R(T)$ - R_0 - BT^5 as a function of T^2 at different pressures.

Appendix B: Normal-State Resistance Fitting and Analysis

Previous studies have shown that quantum critical behavior can be accompanied by non-Fermi-liquid (NFL) transport [59, 60]. To examine this possibility, we fitted the normal-state resistance in the range of approximately 10-50 K using $R(T) = R_0 + AT^2 + BT^5$, where R_0, A, and B represent the residual resistance and the electron-electron and electron-phonon scattering contributions, respectively. As shown in Fig. A2(a, b), $R(T)$ - R_0 - BT^5 exhibits an approximately linear dependence on T^2 over the investigated pressure range, indicating predominantly Fermi-liquid-like transport. Moreover, as shown in Fig. A3, A decreases overall with pressure and shows no pronounced enhancement near 5 GPa, while R_0 evolves smoothly. Therefore, our normal-state transport data show no clear evidence for a critical enhancement associated with quantum-critical fluctuations; the interplay between SC and CDW may favor phase competition.

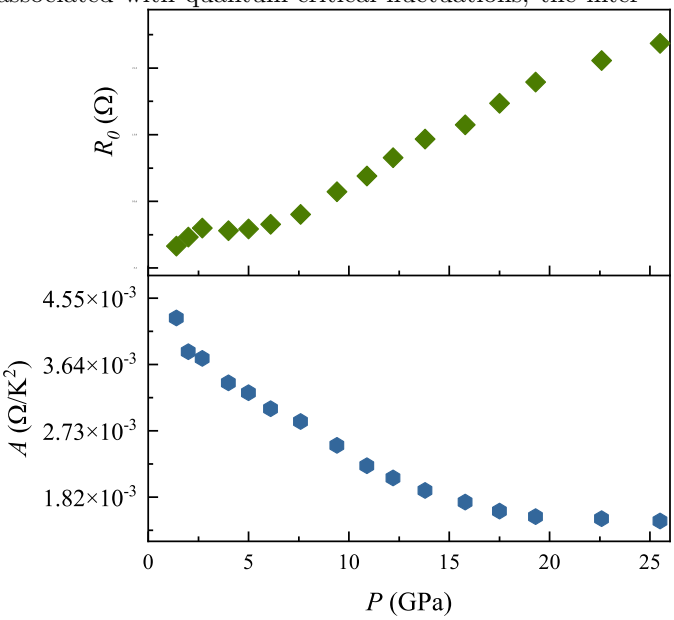


FIG. A3. Pressure dependence of the fitting parameters R_0 and A.

ACKNOWLEDGMENTS

Work at HPSTAR was supported by NSAF, Grant No. U1530402.

* hong.xiao@hpstar.ac.cn † chuanlong.lin@hpstar.ac.cn

[1] Novoselov K S, Geim A K, Morozov S V, Jiang D e, Zhang Y, Dubonos S V, Grigorieva I V and Firsov A A 2004 *science* **306** 666–669 URL https://www.science.org/doi/abs/10.1126/science.1102896

[2] Castro Neto A H, Guinea F, Peres N M R, Novoselov K S and Geim A K 2009 *Rev. Mod. Phys.* **81**(1) 109–162 URL https://link.aps.org/doi/10.1103/RevModPhys.81.109

[3] Bolotin K, Sikes K, Jiang Z, Klima M, Fudenberg G, Hone J, Kim P and Stormer H 2008 *Solid State Communications* **146** 351–355 ISSN 0038-1098 URL https://www.sciencedirect.com/science/article/pii/S0038109808001178

[4] Reyren N, Thiel S, Caviglia A, Kourkoutis L F, Hammerl G, Richter C, Schneider C W, Kopp T, Ruetschi A S, Jaccard D *et al.* 2007 *Science* **317** 1196–1199 URL https://www.science.org/doi/abs/10.1126/science.1146006

[5] Dalrymple B J and Prober D 1984 *Journal of low tem-*

perature physics **56** 545–574
[6] Saito Y, Nojima T and Iwasa Y 2016 *Nature Reviews Materials* **2** 1–18 URL https://doi.org/10.1038/natrevmats.2016.94
[7] Zhang R, Waters J, Geim A K and Grigorieva I V 2017 *Nature communications* **8** 15036 URL https://doi.org/10.1038/ncomms15036
[8] Cao Y, Fatemi V, Fang S, Watanabe K, Taniguchi T, Kaxiras E and Jarillo-Herrero P 2018 *Nature* **556** 43–50 URL https://doi.org/10.1038/nature26160
[9] Lu J, Zheliuk O, Leermakers I, Yuan N F, Zeitler U, Law K T and Ye J 2015 *Science* **350** 1353–1357 URL https://www.science.org/doi/abs/10.1126/science.aab2277
[10] Xi X, Wang Z, Zhao W, Park J H, Law K T, Berger H, Forró L, Shan J and Mak K F 2016 *Nature Physics* **12** 139–143 URL https://doi.org/10.1038/nphys3538
[11] Huang B, Clark G, Navarro-Moratalla E, Klein D R, Cheng R, Seyler K L, Zhong D, Schmidgall E, McGuire M A, Cobden D H *et al.* 2017 *Nature* **546** 270–273 URL https://doi.org/10.1038/nature22391
[12] Tang S, Zhang C, Wong D, Pedramrazi Z, Tsai H Z, Jia C, Moritz B, Claassen M, Ryu H, Kahn S *et al.* 2017 *Nature Physics* **13** 683–687 URL https://doi.org/10.1038/nphys4174
[13] Straub T, Finteis T, Claessen R, Steiner P, Hüfner S, Blaha P, Oglesby C S and Bucher E 1999 *Phys. Rev. Lett.* **82**(22) 4504–4507 URL https://link.aps.org/doi/10.1103/PhysRevLett.82.4504
[14] Yokoya T, Kiss T, Chainani A, Shin S, Nohara M and Takagi H 2001 *Science* **294** 2518–2520 URL https://www.science.org/doi/abs/10.1126/science.1065068
[15] Valla T, Fedorov A V, Johnson P D, Glans P A, McGuinness C, Smith K E, Andrei E Y and Berger H 2004 *Phys. Rev. Lett.* **92**(8) 086401 URL https://link.aps.org/doi/10.1103/PhysRevLett.92.086401
[16] Berthier C, Molinié P and Jérome D 1976 *Solid State Communications* **18** 1393–1395 ISSN 0038-1098 URL https://www.sciencedirect.com/science/article/pii/0038109876909868
[17] Castro Neto A H 2001 *Phys. Rev. Lett.* **86**(19) 4382–4385 URL https://link.aps.org/doi/10.1103/PhysRevLett.86.4382
[18] Inosov D S, Zabolotnyy V B, Evtushinsky D V, Kordyuk A A, Büchner B, Follath R, Berger H and Borisenko S V 2008 *New Journal of Physics* **10** 125027 URL https://dx.doi.org/10.1088/1367-2630/10/12/125027
[19] Moncton D E, Axe J D and DiSalvo F J 1975 *Phys. Rev. Lett.* **34**(12) 734–737 URL https://link.aps.org/doi/10.1103/PhysRevLett.34.734
[20] Harper J, Geballe T and Di Salvo F 1975 *Physics Letters A* **54** 27–28 ISSN 0375-9601 URL https://www.sciencedirect.com/science/article/pii/0375960175905927
[21] Suderow H, Tissen V G, Brison J P, Martínez J L and Vieira S 2005 *Phys. Rev. Lett.* **95**(11) 117006 URL https://link.aps.org/doi/10.1103/PhysRevLett.95.117006
[22] Xi X, Zhao L, Wang Z, Berger H, Forró L, Shan J and Mak K F 2015 *Nature nanotechnology* **10** 765–769 URL https://doi.org/10.1038/nnano.2015.143
[23] Mao H K and Bell P M 1981 *Review of Scientific Instruments* **52** 615–616 ISSN 0034-6748 URL https://doi.org/10.1063/1.1136650
[24] Grzybowski T A and Ruoff A L 1984 *Phys. Rev. Lett.* **53**(5) 489–492 URL https://link.aps.org/doi/10.1103/PhysRevLett.53.489
[25] Hemmes H, Driessen A, Kos J, Mul F A, Griessen R, Caro J and Radelaar S 1989 *Review of Scientific Instruments* **60** 474–480 ISSN 0034-6748 URL https://doi.org/10.1063/1.1140402
[26] Gao C, Han Y, Ma Y, White A, Liu H, Luo J, Li M, He C, Hao A, Huang X, Pan Y and Zou G 2005 *Review of Scientific Instruments* **76** 083912 ISSN 0034-6748 URL https://doi.org/10.1063/1.2006347
[27] Li M, Gao C, Ma Y, Wang D, Li Y and Liu J 2007 *Applied Physics Letters* **90** 113507 ISSN 0003-6951 URL https://doi.org/10.1063/1.2712811
[28] Li Y, Gao Y, Han Y, Liu C, Peng G, Wang Q, Ke F, Ma Y and Gao C 2015 *Applied Physics Letters* **107** 142103 ISSN 0003-6951 URL https://doi.org/10.1063/1.4932525
[29] Welzel O P and Grosche F M 2011 *Review of Scientific Instruments* **82** 033901 ISSN 0034-6748 URL https://doi.org/10.1063/1.3541793
[30] Matsumoto R, Sasama Y, Fujioka M, Irifune T, Tanaka M, Yamaguchi T, Takeya H and Takano Y 2016 *Review of Scientific Instruments* **87** 076103 ISSN 0034-6748 URL https://doi.org/10.1063/1.4959154
[31] Adachi S, Matsumoto R, Yamamoto S, Yamamoto T D, Terashima K, Saito Y, Esparza Echevarria M, Baptista de Castro P, Song P, Iwasaki S, Takeya H and Takano Y 2020 *Applied Physics Letters* **116** 223506 ISSN 0003-6951 URL https://doi.org/10.1063/5.0004973
[32] Chen Y, Ke F, Ci P, Ko C, Park T, Saremi S, Liu H, Lee Y, Suh J, Martin L W, Ager J W, Chen B and Wu J 2017 *Nano Letters* **17** 194–199 pMID: 27935309 URL https://doi.org/10.1021/acs.nanolett.6b03785
[33] Ke F, Chen Y, Yin K, Yan J, Zhang H, Liu Z, Tse J S, Wu J, kwang Mao H and Chen B 2019 *Proceedings of the National Academy of Sciences* **116** 9186–9190 URL https://www.pnas.org/doi/abs/10.1073/pnas.1820890116
[34] Gao Y, Lin X, Smart T, Ci P, Watanabe K, Taniguchi T, Jeanloz R, Ni J and Wu J 2020 *Phys. Rev. Lett.* **125**(22) 226403 URL https://link.aps.org/doi/10.1103/PhysRevLett.125.226403
[35] Xie J, Liu X, Zhang W, Wong S M, Zhou X, Zhao Y, Wang S, Lai K T and Goh S K 2021 *Nano Letters* **21** 9310–9317 URL https://doi.org/10.1021/acs.nanolett.1c03508
[36] Ku C h, Liu X, Xie J, Zhang W, Lam S T, Chen Y, Zhou X, Zhao Y, Wang S, Yang S, Lai K T and Goh S K 2022 *Review of Scientific Instruments* **93** 083912 ISSN 0034-6748 URL https://doi.org/10.1063/5.0098226
[37] Zhang W, Liu X, Wang L, Tsang C W, Wang Z, Lam S T, Wang W, Xie J, Zhou X, Zhao Y, Wang S, Tallon J, Lai K T and Goh S K 2023 *Nano Letters* **23** 872–879 pMID: 36662599 URL https://doi.org/10.1021/acs.nanolett.2c04103
[38] Cao Y, Wang X, Lin X, Yang W, Lv C, Lu Y, Zhang Y and Zhao W 2020 *IEEE Access* **8** 70488–70495
[39] Zhang C, Hu T, Wang T, Wu Y, Yu A, Chu J, Zhang H, Zhang X, Xiao H, Peng W, Di Z, Qiao S and Mu G 2021 *2D Materials* **8** 025024 URL https://dx.doi.org/10.1088/2053-1583/abdaba
[40] Blessing R H 1995 *Acta Crystallographica Section A* **51** 33–38 URL https://doi.org/10.1107/S0108767394005726

[41] Krause L, Herbst-Irmer R and Stalke D 2015 *Journal of Applied Crystallography* **48** 1907–1913 URL https://doi.org/10.1107/S1600576715020440

[42] Sheldrick G M 2015 *Acta Crystallographica Section A* **71** 3–8 URL https://doi.org/10.1107/S2053273314026370

[43] Sheldrick G M 2015 *Acta Crystallographica Section C* **71** 3–8 URL https://doi.org/10.1107/S2053229614024218

[44] van der PAUW L J 1991 *A METHOD OF MEASURING SPECIFIC RESISTIVITY AND HALL EFFECT OF DISCS OF ARBITRARY SHAPE* pp 174–182

[45] Momma K and Izumi F 2011 *Journal of Applied Crystallography* **44** 1272–1276 URL https://doi.org/10.1107/S0021889811038970

[46] Cao Z Y, Zhang K, Goncharov A F, Yang X J, Xu Z A and Chen X J 2023 *Phys. Rev. B* **107**(24) 245125 URL https://link.aps.org/doi/10.1103/PhysRevB.107.245125

[47] Moulding O, Osmond I, Flicker F, Muramatsu T and Friedemann S 2020 *Phys. Rev. Res.* **2**(4) 043392 URL https://link.aps.org/doi/10.1103/PhysRevResearch.2.043392

[48] Naito M and Tanaka S 1982 *Journal of the Physical Society of Japan* **51** 219–227 URL https://doi.org/10.1143/JPSJ.51.219

[49] jun Li L, an Xu Z, qin Shen J, min Qiu L and hua Gan Z 2005 *Journal of Physics: Condensed Matter* **17** 493 URL https://dx.doi.org/10.1088/0953-8984/17/3/008

[50] Khestanova E, Birkbeck J, Zhu M, Cao Y, Yu G L, Ghazaryan D, Yin J, Berger H, Forró L, Taniguchi T, Watanabe K, Gorbachev R V, Mishchenko A, Geim A K and Grigorieva I V 2018 *Nano Letters* **18** 2623–2629 URL https://doi.org/10.1021/acs.nanolett.8b00443

[51] Xing Y, Zhao K, Shan P, Zheng F, Zhang Y, Fu H, Liu Y, Tian M, Xi C, Liu H, Feng J, Lin X, Ji S, Chen X, Xue Q K and Wang J 2017 *Nano Letters* **17** 6802–6807 URL https://doi.org/10.1021/acs.nanolett.7b03026

[52] Smith T F, Delong L E, Moodenbough A R, Geballe T H and Schwall R E 1972 *Journal of Physics C: Solid State Physics* **5** L230 URL https://dx.doi.org/10.1088/0022-3719/5/16/008

[53] Chen K Y, Wang N N, Yin Q W, Gu Y H, Jiang K, Tu Z J, Gong C S, Uwatoko Y, Sun J P, Lei H C, Hu J P and Cheng J G 2021 *Phys. Rev. Lett.* **126**(24) 247001 URL https://link.aps.org/doi/10.1103/PhysRevLett.126.247001

[54] Xu S, Gao J, Liu Z, Chen K, Yang P, Tian S, Gong C, Sun J, Xue M, Gouchi J, Luo X, Sun Y, Uwatoko Y, Lei H, Wang B and Cheng J 2021 *Phys. Rev. B* **103**(22) 224509 URL https://link.aps.org/doi/10.1103/PhysRevB.103.224509

[55] Monteverde M, Lorenzana J, Monceau P and Núñez Regueiro M 2013 *Phys. Rev. B* **88**(18) 180504 URL https://link.aps.org/doi/10.1103/PhysRevB.88.180504

[56] Shen B, Du F, Li R, Thamizhavel A, Smidman M, Nie Z Y, Luo S S, Le T, Hossain Z and Yuan H Q 2020 *Phys. Rev. B* **101**(14) 144501 URL https://link.aps.org/doi/10.1103/PhysRevB.101.144501

[57] Guo C Y, Jiang W B, Smidman M, Han F, Malliakas C D, Shen B, Wang Y F, Chen Y, Lu X, Kanatzidis M G and Yuan H Q 2016 *Phys. Rev. B* **94**(18) 184506 URL https://link.aps.org/doi/10.1103/PhysRevB.94.184506

[58] Du F, Su H, Luo S S, Shen B, Nie Z Y, Yin L C, Chen Y, Li R, Smidman M and Yuan H Q 2020 *Phys. Rev. B* **102**(14) 144510 URL https://link.aps.org/doi/10.1103/PhysRevB.102.144510

[59] Du F, Luo S, Ortiz B R, Chen Y, Duan W, Zhang D, Lu X, Wilson S D, Song Y and Yuan H 2021 *Phys. Rev. B* **103**(22) L220504 URL https://link.aps.org/doi/10.1103/PhysRevB.103.L220504

[60] Shibauchi T, Carrington A and Matsuda Y 2014 *Annual Review of Condensed Matter Physics* **5** 113–135 ISSN 1947-5462 URL https://www.annualreviews.org/content/journals/10.1146/annurev-conmatphys-031113-133921

[61] Chu C W, Diatschenko V, Huang C Y and DiSalvo F J 1977 *Phys. Rev. B* **15**(3) 1340–1342 URL https://link.aps.org/doi/10.1103/PhysRevB.15.1340

[62] Iwaya K, Hanaguri T, Koizumi A, Takaki K, Maeda A and Kitazawa K 2003 *Physica B: Condensed Matter* **329-333** 1598–1599 ISSN 0921-4526 proceedings of the 23rd International Conference on Low Temperature Physics URL https://www.sciencedirect.com/science/article/pii/S0921452602023098